

A Morphological Filter-based Local Prediction Method with Multi-variable Inputs for Short-Term Load Forecast

X. Z. Ye, T. Y. Ji*, *IEEE Member*, M. S. Li, *IEEE Member*, Q. H. Wu, *IEEE Fellow*

Abstract—This paper presents a prediction model for short-term electric load forecast based on Local Prediction (LP) with a dual-SE weighted morphological filter derived from Mathematical Morphology (MFLP). The historical load data with frequent fluctuations is processed by a morphological filter to obtain a relatively smooth load curve and meanwhile reserve the characteristics of the load. After filtering out the volatility, the obtained time series is embedded into a high-dimension phase space by the LP. Moreover, weather conditions such as local temperature and humidity can also be involved in the proposed MFLP, by embedding them as an individual temperature series and a weather series, respectively, to form a forecast sample. The nearest neighbours who have high similarity to the forecast sample are selected to construct the training set and then predicted by Support Vector Regression (SVR). In order to evaluate the performance of the proposed model, simulation studies have been carried out, respectively, on data collected by AEMO and Elia, in comparison with the SVR, Back Propagation Neural Network (BPNN) and persistence (Per.) models. The results demonstrate that the accuracy and stability of the proposed model are much better than the traditional models.

Index Terms—Morphological filter, local prediction, load forecast, multi-variable inputs

I. INTRODUCTION

With the deregulation of electricity industry and construction of electricity market, the whole electricity sector has been undergoing record decades. The reform brings an open electricity market for market participants. At the same time, with the development of smart grid, modern technologies such as communication technology have been penetrated into the electricity grid [1]. The electricity industry is not the traditional one anymore, and the electricity market brings harsh competition to all market participants. Each market participant is an individual seeking for maximizing profit. In such situation, timely and accurate load forecast is urgently needed by system operators, suppliers, power generators, etc, to optimize system and market operation, enhance system security, minimize transmission loss, optimize demand side management, etc [2] [3]. Thus, load forecast plays an even more important role in the competitive environment [4].

According to time scale, load forecast can be classified into several categories: long-term, medium-term, short-term and

The project is supported by Guangdong Innovative Research Team Program (No. 201001N0104744201).

The authors are with the School of Electric Power Engineering, South China University of Technology (SCUT), Guangzhou, 510641, China. Corresponding author: Dr. T. Y. Ji, Email: tjji@scut.edu.cn.

ultra-short-term prediction. The latter two types deal with the prediction from one hour up to a few days [5] offering decision basis for pre-scheduling plan, real-time scheduling, real-time electricity price forecasting. In many countries, the time interval between short-term dispatch actions is very short [6]. One data set in this paper comes from Australia where the time interval is only 5 minutes. In such cases, load forecast is concerned with both time consumption and accuracy.

Many data-driven mathematical statistics approaches and artificial intelligence approaches have been proposed in the field of forecast. Several well-known data-driven approaches include the Per. model [7], artificial neural network (ANN) [8], autoregressive and moving average (ARMA) [9], support vector machine (SVM) [10], and a number of methods have been proposed on this basis. The Per. model is a kind of simple but non-intelligent model [7]. With the development of artificial intelligence forecasting techniques, the ANNs are recognized as powerful tools for prediction [8]. But its forecast accuracy relies on the huge amount size of training samples. The ARMA [9] techniques are criticized for its incapability when dealing with non-linear problems. In many cases SVM [11] gets satisfactory results but once the parameters are not properly tuned, the result may go wild. The SVR [12] is derived from the SVM. The kernel functions of SVR help it to achieve non-linear mapping from the sample space to the feature space successfully. Since it provides a better performance in high-variance time series prediction, the SVR has been adopted widely in the field of forecast.

Nonetheless, the time consumption of the conventional model is usually large which reduces the prediction efficiency especially in short-term forecast. Furthermore, electrical load is related closely to complex demand side behaviours. Hence, using the previous models to forecast directly is not acceptable. A number of approaches to forecast electric load is developed. Models decompose the load into several components have been proposed by researchers such as wavelet transformation (WT) [13] and empirical mode decomposition (EMD) [14] [15]. Nevertheless, decomposing the original time series into several components and forecasting them respectively may bring errors in every component and cause the increases of total error, so that the final result is far from satisfactory. In another word, the stochastic component which indicates the high randomness of human behaviours is unpredictable. Therefore, a MM-based filter is proposed aiming at filtering out this kind of component.

Electrical load is mainly classified into three categories—industrial, commercial, residential. The characteristics of commercial and residential load depend on weather to a certain extent. In conventional methods, only the historical load data is used to construct the training set. Nonetheless, this paper also engages weather data in prediction to make full use of weather information to improve forecast accuracy. In fact, the reliability of forecast is sensitive to the internal relevances between the forecast point and its nearest neighbours. The proposed model engages multi-variables can select the nearest neighbours those carry the maximal relevance.

This paper proposes a novel model for short-term load forecast. The morphological filter is used to filter out the stochastic component of original load curve and reserve the characteristics of the load. The filtered load data and the weather data in time series are embedded together into a high dimension phase space by the LP. The SVR is applied to perform the forecast using the training data set selected by the LP.

II. A FILTER BASED ON MATHEMATICAL MORPHOLOGY

A. Mathematical morphology (MM)

MM as a signal/image processing technique is proposed based on integral geometry and random set theory, which is quite different from frequency domain filtering methods. In this paper, it is used to deal with load data which is a time series. The local features of the load curve reflect the behavior of demand side which should not be ignored. The proposed MM-based filter reserves these features well, and improves forecast accuracy and stability greatly.

All the MM operators are derived from two basic operations, dilation and erosion [16]. A one-dimension signal $f(k)$ dilated or eroded by a structuring element (SE) $g(s)$ are, respectively, defined as follows:

$$f \oplus g(k) = \max\{f(k-s) + g(s)\} \quad (1)$$

$$f \ominus g(k) = \min\{f(k+s) - g(s)\} \quad (2)$$

For all k and s , they must satisfy $0 \leq (k-s) \leq k$ and $0 \leq (k+s) \leq k$, respectively, in (1) and (2).

The opening and closing operations are, respectively, defined as follows:

$$(f \circ g)(k) = f \ominus g \oplus g(k) \quad (3)$$

$$(f \bullet g)(k) = f \oplus g \ominus g(k) \quad (4)$$

where \circ and \bullet denote the opening and closing operation respectively. Generally, the opening operation is used to eliminate the scattered points which smoothes and inhibits the peak noise and the closing operation is used to connect the two adjacent areas which inhibits the negative low noise.

Variable combinations of dilation, erosion, opening and closing operations construct different filters and achieve different signal processing results.

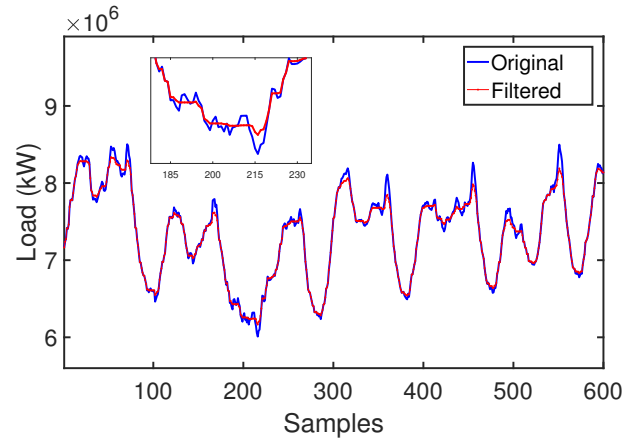


Fig. 1: Filtering result of the proposed morphological filter

B. A novel morphological filter

In order to obtain relatively smoother curve which reserves the useful information of the original load data, a new filter has been proposed in this paper based on the open-closing and close-opening filters. The dual-SE weighted morphological filter is defined as follows:

$$F(k) = \lambda_1(f \circ g1 \bullet g2)(k) + \lambda_2(f \bullet g1 \circ g2)(k) \quad (5)$$

where f is the signal to be processed; λ_1, λ_2 are the weighted coefficients, and $\lambda_1 + \lambda_2 = 1$; $g1$ and $g2$ are SEs of different shapes; $g1$ is a flat SE while $g2$ is a disc shape one. The value of λ_1 is set to be 0.3 and λ_2 is set to be 0.7 after a great number of tests.

The original load curve has a certain periodicity. However, the rapidly changing stochastic component is non-predictable. Thus, a flat SE named $g1$ is used to deal with them and get a relatively smooth curve. After the process by $g1$, the characteristics of the curve are not as same as before. To filter out the stochastic component completely, a disc shape SE named $g2$ is used on the obtain curve. Finally, the filtering result is used for forecasting and ensures a better performance.

Fig. 1 illustrates the result of original load curve processed by the morphological filter. When the load is high, the stochastic component that should be regarded as interference is filtered out and the curve reserves the wave trend of the peak load. When the load is low, the curve retains the characteristics of the original load curve.

III. LOCAL PREDICTION METHOD

Unlike global prediction, LP selects part of historical data to be used for setting up training set, instead of engaging all the historical data. LP identifies local pattern for each point, which is unique and can be displayed in a more obvious manner in a high-dimension space. Therefore, LP is more targeted in the modeling stage, leading to a high accuracy than global prediction.

A. The principle of local prediction (LP)

Take a three-dimension phase space for example. The principle of local predictor is illustrated in Fig. 2. The original time series is embedded into the three-dimension phase space and forms a batch of samples. LP chooses a set of nearest neighbours, named local neighbours, who have smaller Euclidean distance to the forecast sample, and the local neighbours possess high similarity to the forecast sample.

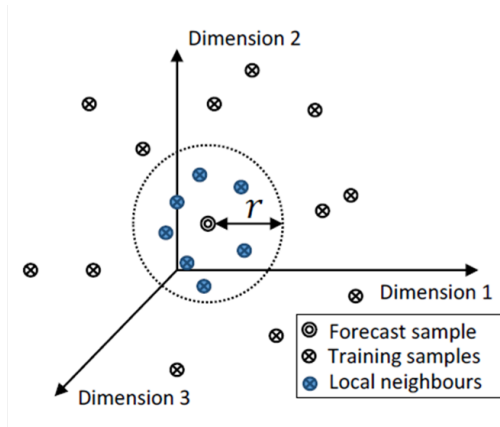


Fig. 2: LP using the local neighbours

B. Constructing the phase space

The historical load data is collected in time series. The data in a univariate time series contains all the information of the variables relatively. In other words, one-dimension time series can be regarded as a lower dimension with compressed information of high dimension. For a high-variance system, the information in the time series can be extracted from one dimension to a higher dimension by reconstructing a new space named the phase space using embedding theorem [17].

In time domain, the sample s_i , $i = 1, 2, \dots, K$ demonstrates the local information where K is the length of the time series. Correspondingly, the phase space can be reconstructed by the delay coordinate, which is defined as:

$$\mathbf{s}_t = [s(t), s(t + \tau), \dots, s(t + (d - 1)\tau)]^T \quad (6)$$

where d denotes the embedding dimension, τ is the time delay constant and T stands for the vector transpose.

All the \mathbf{s}_t are independent points in the phase space, and they jointly form a matrix of:

$$\mathbf{S} = [\mathbf{s}_1, \mathbf{s}_2, \dots, \mathbf{s}_q]^T \quad (7)$$

where $q = L - (d - 1)\tau$.

To illustrate information in one-dimension time domain to a maximum degree, it is of great importance to determine the embedding dimension d and the time delay τ .

C. Estimate embedding dimension d and time delay τ

According to the delay coordinate, the phase space reconstructed is a d -dimension space and the obtained series is a reconstructed embedded series containing the information of the one-dimension time series as much as possible.

1) The embedding dimension d :

As for load forecast, the fundamental of feature selection technique is to maximize relevancy, minimize redundancy and maximize synergy [18]. The embedding dimension of the new reconstructed phase space is relatively large, satisfying the following formulae:

$$d = 2 \cdot \lceil \text{boxdim}(\mathbf{A}) \rceil + 1 \quad (8)$$

where $\text{boxdim}(\mathbf{A})$ is the dynamic system attractor. To formulate the system dimension, the correlation dimension d_c is determined from the correlation integral which is defined as follows:

$$C(r) = \lim_{N \rightarrow \infty} \frac{1}{N} \sum_{i=1}^N \sum_{j=1}^N \theta(r - \|(X_i) - (X_j)\|), (i \neq j) \quad (9)$$

where $\theta(x)$ is the Heaviside step function defined as:

$$\theta(x) = \begin{cases} 0, & x \leq 0 \\ 1, & x \geq 0 \end{cases} \quad (10)$$

Obviously, the value of $C(r)$ depends on the size comparison of r and $\|(X_i) - (X_j)\|$ as follows:

$$C(r) = \begin{cases} 0, & r \leq \|(X_i) - (X_j)\| \\ 1, & r \geq \|(X_i) - (X_j)\| \end{cases} \quad (11)$$

Thus, it is important to choose an appropriate r . When $r \rightarrow 0$, the following equation gives the correlation dimension d_c :

$$d_c = \lim_{r \rightarrow 0} \frac{\lg C(r)}{\lg(r)} \quad (12)$$

Therefore, the embedding dimension d can be obtained by $d = \lceil (2d_c + 1) \rceil$ as mentioned in (8).

2) The time delay τ :

To estimate the best selection of the time delay τ , average displacement is adopted.

The vector \mathbf{s}_i , $i = 1, \dots, q$ in the phase space can be constructed by the time series $s(t)$ according to (6). Thus, the average distance of two adjacent points can be defined as:

$$D_d(\tau) = \frac{1}{q} \sum_{i=1}^q \|\mathbf{s}_{i+\tau} - \mathbf{s}_i\| \quad (13)$$

Then the formula of average distance can be obtained:

$$D_d(\tau) = \frac{1}{q} \sum_{i=1}^q \left[\sum_{j=1}^{d-1} (\mathbf{s}_{i+\tau} - \mathbf{s}_i)^2 \right]^{\frac{1}{2}} \quad (14)$$

With the gradual increase of τ , $D_d(\tau)$ will increase linearly until getting saturated when $\partial D_d / \partial \tau = 0$. The τ corresponding to the end of its linear region is the best time delay.

D. Local prediction (LP) method

The first step of LP method is to select a set of nearest neighbours with high similarity to the forecast sample in the phase space. Take one point \mathbf{s}_r as an example. Searching for the k -neighborhood of \mathbf{s}_r is to find all the points in the δ region. The δ region is a hyper sphere with \mathbf{s}_r as the center and δ as

the radius. The k -neighborhood of \mathbf{s}_r is labeled as $\mathbf{s}_{r(j)}$, where $j = 1, 2, \dots, k$ and $\mathbf{s}_{r(j)}$ must satisfy the following inequality:

$$\|\mathbf{s}_r - \mathbf{s}_{r(j)}\| < \delta \quad (15)$$

$\|\mathbf{s}_r - \mathbf{s}_{r(j)}\|$ stands for the Euclidean distance in the phase space which is defined as:

$$\|\mathbf{s}_r - \mathbf{s}_{r(j)}\| = \sqrt{\sum_{t=1}^N [s_r(t) - s_{r(j)}(t)]^2} \quad (16)$$

The training set \mathbf{T}_r used to obtain the forecast model by training SVR model can be constructed as:

$$\mathbf{T}_r = [\mathbf{s}_{r(1)}, \mathbf{s}_{r(2)}, \dots, \mathbf{s}_{r(k)}] \quad (17)$$

After that the forecast results can be got easily.

IV. CASE STUDIES

A. Data used in this paper

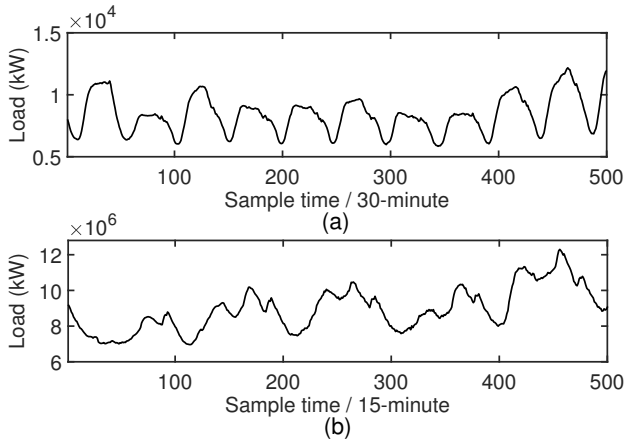


Fig. 3: Data from the two data sets: (a) Sydney; (b) Elia.

Simulation studies are conducted using two data sets from AEMO located in Australia and Elia located in Belgium, respectively. The former data set sampled once every 30 minutes from 1st January, 2006 to 1st January, 2011 is labeled as Set 1. As weather condition such as temperature has great impact on the load especially in summer, weather data should also be employed for load forecast. Therefore, Set 1 includes the weather data provided by Sydney Observatory from the BOM including humidity, the dry bulb, the wet bulb, the dew point temperature. The latter data set sampled once every 15 minutes from 1st January, 2013 to 1st April, 2017 is labeled as Set 2. In order to verify the performance of the forecast models, the load data in January, March, May, July, September and November are forecasted and compared with actual data. The load data of the two data sets are illustrated in Fig. 3.

B. Performance qualification

To evaluate the performance quality of MFLP model, the mean absolute percentage error (MAPE) and the normalized mean absolute error (NMAE) are applied in this paper. Both of them assess the forecast accuracy by comparing the forecast value and the actual value, and smaller MAPE and NMAE indicate better forecast results. These two evaluation measures are defined, respectively, as follows:

$$\text{MAPE} = \frac{1}{N} \sum_{i=1}^N \frac{|y_i - \hat{y}_i|}{y_i} \times 100\% \quad (18)$$

$$\text{NMAE} = \frac{1}{N} \sum_{i=1}^N \frac{|y_i - \hat{y}_i|}{P_{\text{inst}}} \times 100\% \quad (19)$$

where N is the size of the forecast set, y_i denotes the actual value, \hat{y}_i stands for the forecast value, and P_{inst} is the maximal value of the historical data.

C. Models employed for comparison

For the purpose of comparing the forecast results, simulation studies are conducted with the Per., BPNN, and SVR models.

The Per. model takes the last measured value as the forecast one. Since its apparent simplicity, the Per. model is usually used as a benchmark for reference. However, its mechanism is non-intelligent. Due to high complexity of the load characteristics, the Per. model is not applicable in practical application in fact.

The BPNN model has been widely used in machine learning and shows good performance in the field of forecast [18]. But the forecast accuracy and stability relies on large amount of data to a great extent.

The SVR model is also widely used in prediction and performs well in many cases. However, the process of searching for the optimal parameters is very time consuming [19], which limits its application especially in short-term forecast.

These three models are mature and recognised by the researchers. Therefore, they are employed in this paper for comparison. Besides, in order to test the effect of the proposed filter, simulation studies are also conducted in comparison with the SVRLP model. The SVRLP model combines the SVR with LP, which improves the forecast speed greatly. However, the nearest neighbors selected by the SVRLP model are original data without filtering out the stochastic component. As a result, the nearest neighbours in the SVRLP model may not have such high similarity as those in the MFLP model.

D. Experimental results and discussion

Simulation studies are carried out in Set 1. The huge amount size of data in Set 1 covers five years which ensures the prediction covers almost all the local situations and increases the persuasiveness of the model. The prediction results of 4-step ahead are shown in Fig. 4, where the forecast curve is almost superposing with the actual curve, indicating an excellent forecast performance. For the purpose of estimating the stability of the forecast model in multi-step, simulations are conducted among the Per., BPNN, SVR, SVRLP and

TABLE I: PERFORMANCE EVALUATION OF FORECAST MODELS ON SET 1 (%)

Methods	1-step ahead		4-step ahead		12-step ahead		20-step ahead	
	MAPE(%)	NMAE(%)	MAPE(%)	NMAE(%)	MAPE(%)	NMAE(%)	MAPE(%)	NMAE(%)
MFLPW	0.3930	0.3877	0.8271	0.6591	1.9490	1.7026	2.8469	2.4105
MFLP	0.4091	0.3971	0.8330	0.7719	2.2455	1.8510	2.8868	2.4149
SVRLP	0.5564	0.4059	1.2248	0.8796	2.9226	2.0595	3.2196	2.3908
SVR	0.6743	0.4198	2.1225	1.2924	4.0062	2.4897	5.0201	3.1457
BP	0.8210	0.5092	2.9284	1.7889	6.1456	3.8438	6.4763	4.0937
Per.	2.4825	1.6313	4.0176	3.9775	9.0176	7.2657	15.1963	9.2259

TABLE II: PERFORMANCE EVALUATION OF FORECAST MODELS ON SET 2 (%)

Methods	1-step ahead		4-step ahead		12-step ahead		20-step ahead	
	MAPE(%)	NMAE(%)	MAPE(%)	NMAE(%)	MAPE(%)	NMAE(%)	MAPE(%)	NMAE(%)
MFLP	0.3415	0.4083	0.5120	0.6051	1.0661	1.2632	1.6022	1.8935
SVRLP	0.4769	0.5555	0.7703	0.8995	1.7572	2.0335	2.6231	2.9917
SVR	0.6861	0.4008	2.3078	1.3362	4.9821	2.8827	6.4454	3.7135
BP	0.6564	0.3901	1.8566	1.1127	4.5957	2.6869	6.1818	3.5473
Per.	1.1022	0.7853	3.6441	2.6061	9.2916	6.5953	13.1400	9.2421

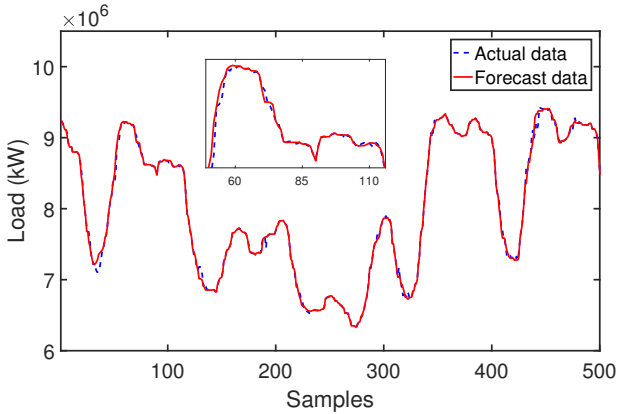


Fig. 4: Prediction results of the MFLP model (4-step ahead) on Set 2

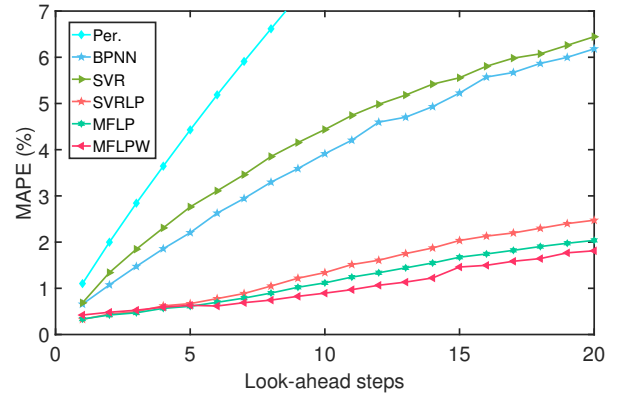


Fig. 5: The MAPEs of the four models on Set 1

MFLP models. In addition, simulations are conducted on the multi-variable inputs MFLP model which considers weather conditions, called MFLPW in this paper. The experimental results are illustrated in Fig. 5 and Fig. 6. Part of MAPEs and NMAEs of the Per. model are not shown. As shown in the figures, the slope of the MAPE and NMAE curves reflects the performance of the models under an increasing forecast step. A smaller slope means that although the forecast step is larger, the accuracy of the forecast model is not degraded much; whereas a higher slope implies that the forecast error rises as the forecast step increases. The slope of both MAPEs and NMAEs of the SVRLP, MFLP and MFLPW models are smaller than that of the Per., BPNN and SVR models in all multi-step cases, indicating that the LP is effective in improving conventional models. At the same time, it is obviously verified that the proposed filter has a positive impact because the performance of MFLP model is better than the SVRLP model. Furthermore, the MAPEs and NMAEs of the MFLPW model are the smallest among

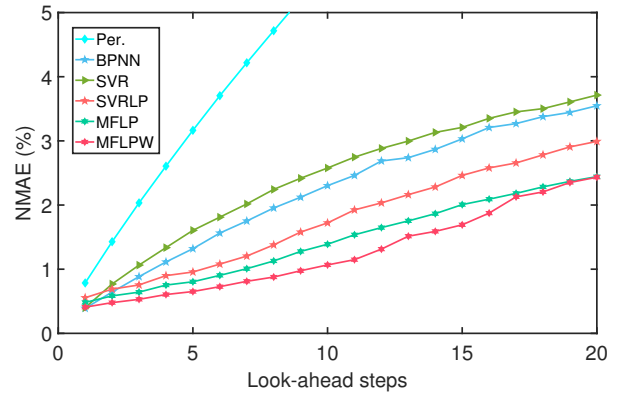


Fig. 6: The NMAEs of the four models on Set 1

all the models. Thus, the weather condition considered method improves the forecast performance of MFLP exactly.

Fig. 7 shows the MAPEs of different models in forecasting

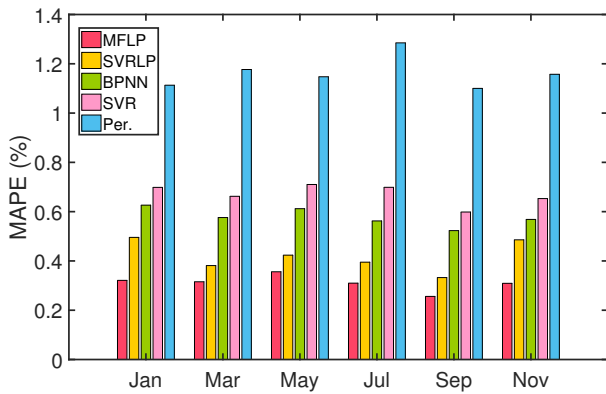


Fig. 7: The monthly MAPE comparison among the Per., BP, SVR, SVRLP and MFLP models (1-step ahead) on Set 2

the load of several typical months. As can be seen in the figure, the MAPEs of all the models are stable in these months while MFLP sustains the lowest level which means the best performance among the five models in all the months covering the whole year.

Simulation studies are conducted on the two data sets respectively to verify the performance of MFLP with the results listed in Table I and Table II. Table I also includes the simulation results of the MFLPW model. As can be seen from both Table I and Table II, the MFLP model is superior no matter how long the forecast step is. In addition, results of the SVRLP model are not as good as those of the MFLP model, which illustrates that the morphological filter employed played a positive effect. Furthermore, as shown in Table I, the forecast results of the MFLPW model is the best among all the models, which shows that the consideration of weather conditions improves the forecast accuracy.

V. CONCLUSION

A forecast model named MFLP has been built in this paper, which is used to forecast the short-term load. A morphological filter is constructed to process the original load data, in order to filter out the stochastic component and reserve the characteristics of the original data. This treatment does great help to the subsequent work. The model combines the traditional SVR with the LP. The LP embeds the data into high dimension and converts the original time series into the phase space. The training samples, which is a set of nearest neighbours to the forecast sample, are selected by the LP with minimal Euclidean distance, which has increased the forecast accuracy and speed. In addition, weather condition is considered in this paper, as the characteristics of the load are related closely to this information. By doing so, the forecast accuracy has improved greatly. The simulation studies carried out on two sets of data have demonstrated that the proposed model shows better performance than other traditional models under up to 20-step ahead conditions.

REFERENCES

- [1] D. Baimel, S. Tapuchi, and N. Baimel, "Smart grid communication technologies- overview, research challenges and opportunities," in *International Symposium on Power Electronics, Electrical Drives, Automation and Motion*, 2016, pp. 116–120.
- [2] F. Bizzarri, M. Bongiorno, A. Brambilla, G. Grusso, and G. S. Gajani, "Model of photovoltaic power plants for performance analysis and production forecast," *Sustainable Energy IEEE Transactions on*, vol. 4, no. 2, pp. 278–285, 2013.
- [3] T. C. Chiu, Y. Y. Shih, A. C. Pang, and C. W. Pai, "Optimized day-ahead pricing with renewable energy demand-side management for smart grids," *IEEE Internet of Things Journal*, vol. PP, no. 99, pp. 1–1, 2016.
- [4] K. Maciejowska and R. Weron, "Short- and mid-term forecasting of baseload electricity prices in the u.k.: The impact of intra-day price relationships and market fundamentals," *IEEE Transactions on Power Systems*, vol. 31, no. 2, pp. 994–1005, 2016.
- [5] G. Dudek, "Artificial immune system for short-term electric load forecasting," *IEEE Transactions on Evolutionary Computation*, vol. PP, no. 99, pp. 1–1, 2016.
- [6] C. Wu, G. Hug, and S. Kar, "Risk-limiting economic dispatch for electricity markets with flexible ramping products," *IEEE Transactions on Power Systems*, pp. 1–14, 2015.
- [7] M. J. Owens, R. Challen, J. Methven, E. Henley, and D. R. Jackson, "A 27 day persistence model of near-earth solar wind conditions: A long lead-time forecast and a benchmark for dynamical models," *Space Weather- the International Journal of Research & Applications*, vol. 11, no. 5, pp. 225–236, 2016.
- [8] L. G. Chen, H. D. Chiang, N. Dong, and R. P. Liu, "Group-based chaos genetic algorithm and non-linear ensemble of neural networks for short-term load forecasting," *Iet Generation Transmission & Distribution*, vol. 10, no. 6, pp. 1440–1447, 2016.
- [9] L. Aggoune, Y. Chetouani, and H. Radjeai, "Change detection in a distillation column using non-linear auto-regressive moving average with exogenous input model and hellinger distance," *Iet Science Measurement & Technology*, vol. 10, no. 1, pp. 10–17, 2015.
- [10] Y. Liu, Y. Sun, D. Infield, Y. Zhao, S. Han, and J. Yan, "A hybrid forecasting method for wind power ramp based on orthogonal test and support vector machine (ot-svm)," *IEEE Transactions on Sustainable Energy*, vol. PP, no. 99, pp. 1–1, 2016.
- [11] H. T. Shiao, V. Cherkassky, J. Lee, B. Veber, N. Patterson, B. Brinkmann, and G. Worrell, "Svm-based system for prediction of epileptic seizures from ieeg signal," *IEEE transactions on bio-medical engineering*, vol. PP, no. 99, pp. 1–1, 2016.
- [12] A. Kavousi-Fard, "Modeling uncertainty in tidal current forecast using prediction interval-based svr," *IEEE Transactions on Sustainable Energy*, vol. PP, no. 99, pp. 1–1, 2016.
- [13] H. Deng, Y. Zhang, and X. G. Duan, "Wavelet transformation-based fuzzy reflex control for prosthetic hands to prevent slip," vol. PP, no. 99, pp. 1–1, 2016.
- [14] L. Ghelardoni, A. Ghio, and D. Anguita, "Energy load forecasting using empirical mode decomposition and support vector regression," *IEEE Transactions on Smart Grid*, vol. 4, no. 4, pp. 549–556, 2013.
- [15] Y. Ren, P. N. Suganthan, and N. Srikanth, "A comparative study of empirical mode decomposition-based short-term wind speed forecasting methods," *IEEE Transactions on Sustainable Energy*, vol. 6, no. 1, pp. 236–244, 2014.
- [16] Q. H. Wu, Z. Lu, and T. Y. Ji, "Protective relaying of power systems using mathematical morphology," vol. 45, 2009.
- [17] P. L. D. Npoli, I. Drelichman, and N. Saintier, "Weighted embedding theorems for radial besov and triebel-lizorkin spaces," *Mathematics*, 2016.
- [18] O. Abedinia, N. Amjady, and H. Zareipour, "A new feature selection technique for load and price forecast of electrical power systems," *IEEE Transactions on Power Systems*, vol. 32, no. 1, pp. 1–1, 2016.
- [19] Y. Xiao, H. Wang, and W. Xu, "Parameter selection of gaussian kernel for one-class svm," *IEEE Transactions on Cybernetics*, vol. 45, no. 5, p. 927, 2014.